

NONLINEAR DYNAMICS OF ELECTROKINETIC INSTABILITIES

Jonathan D. Posner[†] and Juan G. Santiago

Department of Mechanical Engineering, Stanford University, Stanford, CA 94305

JONATHAN.POSNER@STANFORD.EDU

ABSTRACT

Electrokinetic instabilities are generated by a coupling of electric fields and ionic conductivity gradients. This coupling results in an electric body force in the bulk liquid that can generate temporal, convective, and absolute flow instabilities. In this work, we perform a parametric experimental study of convective instabilities in cross-shaped microchannels using epifluorescence microscopy and high speed digital imaging. We report temporal power spectra and spatiotemporal maps as a function of the applied field. The spectral analyses reveal that disturbances induced by electrokinetic instability are purely sinusoidal at the onset of instability and exhibit higher-order harmonics, frequency bifurcations, and continuous power spectra with increasing electric Rayleigh number. Electrokinetic instabilities (EKI) in cross-shaped channels are relevant to injections for field amplified sample stacking, electrokinetic flows at the intersections in multi-dimensional assay devices, and systems with indeterminate sample chemistry.

INTRODUCTION

Electrokinetic instabilities (EKI) are caused by a coupling of electric fields and ionic conductivity gradients. The coupling of an electric field and a conductivity gradient results in an electric body force (per unit volume) of the form, $(\varepsilon \bar{E} \cdot \nabla \sigma) \bar{E}$ where ε , \bar{E} , and σ are the local values of permittivity, electric field, and ionic conductivity, respectively. This coupling results in an electric body force in the bulk liquid, outside the electric double layer, that can generate temporal, convective, and

absolute flow instabilities. Electrokinetic flows with conductivity gradients become unstable when the electroviscous stretching and folding of conductivity interfaces grows faster than the dissipative effect of molecular diffusion¹. EKI's are relevant to on-chip electrokinetic flows with conductivity gradients such as field amplified sample stacking², flow at the intersections of multi-dimensional assays³, electrokinetic control and separation of sample streams with poorly specified chemistry, and low-Reynolds number micromixing⁴.

We have presented detailed EKI models of temporal instabilities in long-thin capillaries for symmetric binary electrolytes^{5,6} and multiple ionic species⁷. Experimental investigations of EKIs include studies of rapid micromixing^{4,8}, visualization of coherent flow structures^{1,9}, and quantitative determination of the critical conditions for instability¹. These studies collectively provide a fundamental understanding of electrokinetic instabilities, identify key controlling parameters, present predictive simulations, and determine the conditions for instability onset. Electrokinetic flows with conductivity gradients become unstable when an electric Rayleigh number is exceeded. In recent work, we showed that electrokinetic flows in cross-shaped channels become unstable when a locally defined electric Rayleigh number exceeds 205¹. The local electric Rayleigh number is defined as,

$$\text{Ra}_{e,\ell} \equiv \frac{\varepsilon E_0^2 d^2}{D \mu} \frac{\gamma - 1}{\gamma} \nabla^* \sigma^* \Big|_{\text{max}},$$

where ε is the fluid permittivity, E_0 is the nominally applied electric field, d is the channel depth, D is the

[†]Presently at Dept. of Mechanical Engineering,
Arizona State University

effective diffusivity of the ions, μ is the fluid viscosity, and $\nabla^* \sigma^* \Big|_{\max}$ is a normalized (to unity) measure of the maximum conductivity gradients in the flow. In this work, we experimentally investigate the nonlinear dynamics of convective electrokinetic instabilities in cross-shaped microchannels over a wide range of electric Rayleigh numbers. The fluid and channel properties remain constant (i.e. ε , d , D , μ γ) and we primarily control the Rayleigh number with the DC applied electric field. E_0 .

RESULTS

We performed experiments in isotropically-etched, cross-pattern microchannels 50 μm wide and 20 μm deep (Micralyne, Alberta, Canada). Instantaneous concentration fields of electrically neutral, rhodamine B dye are captured using epifluorescence microscopy and high speed CCD camera imaging. We use 10 mM HEPES buffered aqueous solutions and add KCl salt to reach the desired conductivities. Details of the experimental setup and conditions are given in Posner and Santiago¹.

Figure 1 shows representative scalar images recorded at five nominally applied fields and a center to sheath ionic conductivity ratio of $\gamma = 100$. The applied field is denoted in above each image. The dyed, high conductivity center stream (40 mS/cm) flows from the west (left) channel and the low conductivity background electrolyte (0.4 mS/cm) sheath streams flow from the north (top) and south (bottom) channels, forming two conductivity interfaces. Temporal power spectra of scalar concentration are shown to the right of each scalar image. At low applied fields the

Rayleigh number remains below the critical value (205) and the flow is stable, as shown in Figure 1a. When a critical electric Rayleigh number is exceeded, sinuous patterns develop and advect downstream resulting in a single spectral peak at $\nu = 42 \text{ sec}^{-1}$, as shown in Figure 1b. As the applied field increases, we observe the disturbances further upstream towards the origin of the conductivity gradients at $x/w = 0$. At these higher fields the power spectra exhibit sub-harmonics and higher-order harmonics (see Figure 1c), frequency bifurcations (see Figures 1c, 1d), and continuous energy spectra (see Figure 1e).

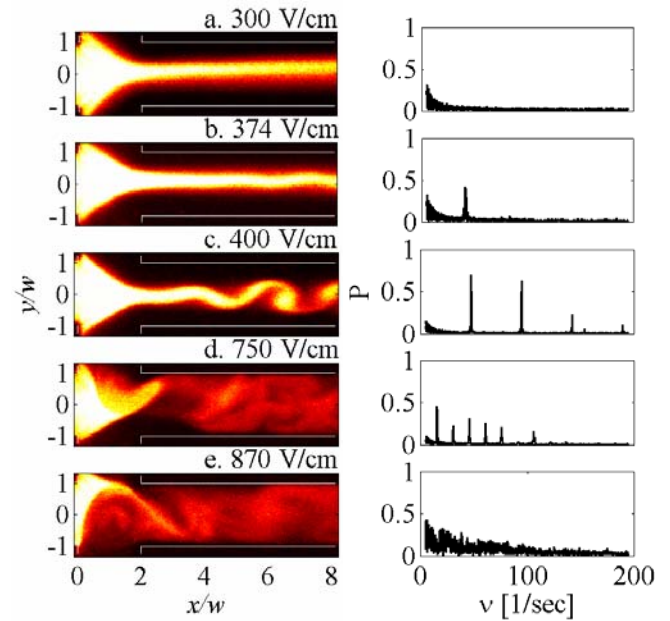


Figure 1. Representative scalar concentration fields of unstable electrokinetic flow in a cross-shaped, 50 μm microchannel. The applied electric field is indicated above each image. For an applied field above a critical value, sinuous patterns develop and advect downstream, as shown in (b). Power spectra of the temporal scalar concentration are shown to the right of each scalar image. For marginally unstable flow, as shown in (b), perturbations are purely sinuous and we observe a single peak at $\nu = 42 \text{ sec}^{-1}$. With a 5 % increase in the applied field (c) three additional harmonics develop. At larger fields, we observe period doubling (d) and then continuous energy spectra (e).

The evolution of the frequency content with increasing applied field is more clearly represented by a temporal spectral map as shown in Figure 2. This map is generated from power spectra similar to those shown in Figure 1 and recorded at 10 V/cm increments. We compute these power spectra (and the ones shown in Figure 1) from time series records extracted from images 3 pixels wide and 512 pixels long recorded at a sampling rate of 390 sec^{-1} . Time series records are composed of the area averaged intensity of a three by three pixel region centered along the x -axis at $x/w = 3$ and $y/w = 0$. We calculate the power spectrums using discrete fast fourier transforms and apply a Hanning window to reduce frequency leakage.

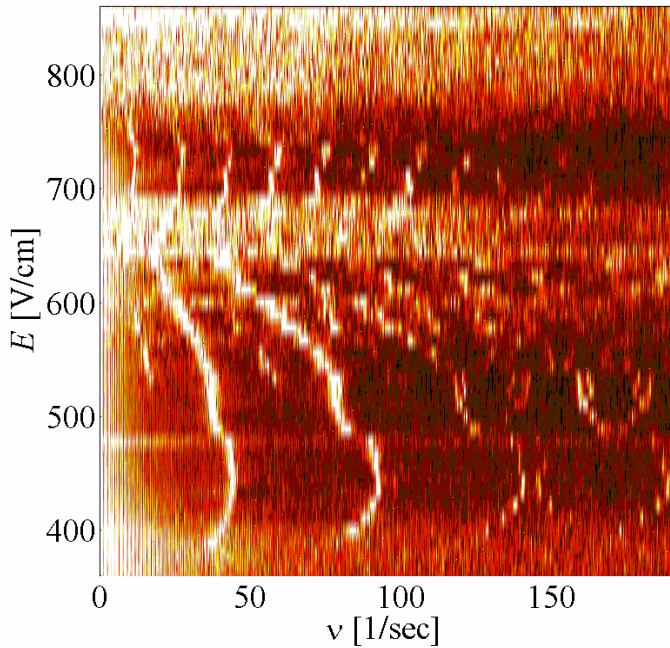


Figure 2. Map of temporal power spectrum as function of nominally applied field. The spectrum is single valued ($\nu=42 \text{ sec}^{-1}$) for marginally unstable flows at the onset of instability $E_a \approx 374 \text{ V/cm}$. At higher applied fields we detect additional harmonics at $\nu=84, 126,$ and 168 sec^{-1} . We observe frequency bifurcations at $E_a=475$ and 650 V/cm . The power spectrum map reveals strong evidence of period doubling at $E_a=530$ and 650 V/cm . Broad frequency content underlies the peaks in the field range of $650 < E_a < 700 \text{ V/cm}$. At fields in excess of $E_a=775 \text{ V/cm}$ well defined frequency peaks cascade into a continuous spectrum.

This spectral map shows that these flows exhibit higher order harmonics, period doubling (i.e., frequency bifurcations), and regions of continuous energy spectra, all of which are consistent with strong nonlinear dynamics and chaos. These flows also exhibit field-dependent regions of aperiodicity and periodicity. For example, there is a region of (periodic) sharp frequency peaks in the range $700 < E_a < 775 \text{ V/cm}$, which is bounded by two regions of (aperiodic) continuous power spectra. Although this data is constructed from temporal records recorded at $x/w = 3$, the spectra look qualitatively similar for records generated at x/w positions less than 8.

Figure 3 shows five spatiotemporal maps of concentration. These are constructed from a sequence of single rows of pixels extracted from the axial centerline

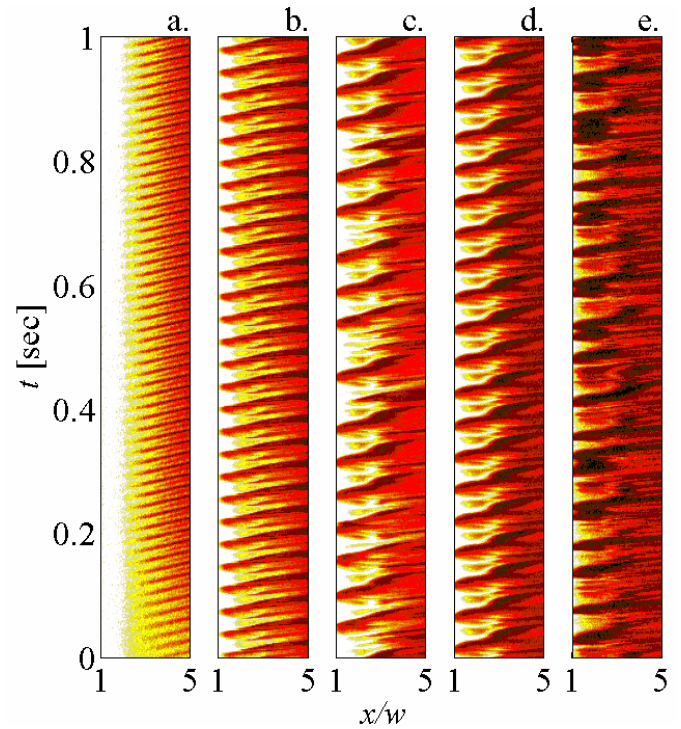


Figure 3. Spatiotemporal maps constructed at four applied fields: a. 388; b. 644; c. 700; d. 722 and e. 844 V/cm. Regularly spaced diagonal lines, as in (a) denote periodic structure formation and a constant downstream advective velocity. At the applied field of $E_a=722 \text{ V/cm}$ (c), there are random events in an otherwise periodic flow. At $E_a=722 \text{ V/cm}$ (e), the flow appears aperiodic over the measured timescale and results in a continuous power spectra.

($y/w = 0$) of scalar images similar to those shown in Figure 1. Regularly spaced, diagonal lines represent periodic structure formation and constant advective velocity. The aperiodic patterns in these maps are representative of stochastic flow structures and consistent with chaotic flow dynamics. Note that at 700 V/cm (Figure 3c) the spatiotemporal map shows some aperiodicity, but when the field is increased to 722 V/cm (Figure 3d) the flow is again periodic. At much higher fields as those shown in Figure 3e the flow appears to be strongly aperiodic.

CONCLUSIONS

We have shown that electrokinetic flows with conductivity gradients become unstable when a critical electric Rayleigh number is exceeded. These flows exhibit both periodic and aperiodic shedding of coherent

scalar structures. Spectral analyses of EKI flows reveal rich physics and dynamic behavior consistent with nonlinear and chaotic systems.

REFERENCES

1. J.D. Posner & J.G. Santiago. 2005. *J. of Fluid Mech.*, *submitted*.
2. B. Jung, R. Bharadwaj, & J.G. Santiago. 2004. *Electrophoresis*, **24**.
3. A. E. Herr, J. I. Molho, K. A. Drouvalakis, J. C. Mikkelsen, P. J. Utz, J. G. Santiago, & T. W. Kenny. 2003. *Anal. Chem.* **75**, 1180
4. M.H. Oddy, J.G. Santiago, & J. C. Mikkelsen, *Anal. Chem.*, 2001, **73**.
5. H. Lin, B. D. Storey, M.H. Oddy, C.H. Chen, & J.G. Santiago. 2004. *Phys. Fluids*, **16**, 6.
6. B.D. Storey, B.S. Tilley, H. Lin, & J.G. Santiago. 2005. **17** *Phys. Fluids*.
7. M. H. Oddy & J. G. Santiago, 2005 *Phys. Fluids*. *In Press*.
8. S.M. Shin, I.S. Kang, Y.-K. Cho, 2005 *J. Micromech. and Microeng.* **15**.
9. C.H. Chen, H. Lin, S.K. Lele, & J.G. Santiago. 2005 *J. of Fluid Mech.*, **524**.